Research Article

Experimental investigation of double-glazed double-pass solar air-heater (DG-DPSAH) with multi-v ribs having trapezoidal roughness geometry

Swati MOR[1] , **Niraj KUMAR[1]** , **Basant SIKARWAR[1],*** , **Gulshan SACHDEVA[2]**

[1]Department of Mechanical Engineering, ASET, Amity University, Noida, Uttar Pradesh, India
[2]Department of Mechanical Engineering, National Institute of Technology, Kurukshetra, Haryana, India

ARTICLE INFO

ABSTRACT

In this study, roughness in the form of multi-V ribs having trapezoidal slots were crafted over the surface of absorber plate for enhancing the heat transfer rate in a solar air heater. An experimental setup was designed and fabricated for demonstrating the performance of this plate with respect to smooth absorber plate. The setup has a double glazed-double pass air flow arrangement. The experiments were conducted under Indian climatic conditions (Latitude = 28.53°N and Longitude = 77.39°E) in September and October 2021 at various rates of air flow through the duct. The results of the roughened absorber plate were compared with the smooth absorber plate. It shows that the multi-V ribs with trapezoidal slots have higher efficacy as compared to smooth absorber plate in the order of 10.42% at an air flow rate of 0.078 kg/s. In addition, the present data of proposed roughness were also compared with data of various roughness available in the literature. It was found that the maximum thermo-hydraulic performance parameter of the proposed roughness texture is higher than other shapes of roughness texture. It was also found that the combination of double-glass cover and double-pass arrangement with the proposed roughness geometry increases the efficiency of the solar air heater at least by one order of the present solar air heating system.

Cite this article as: Mor S, Kumar N, Sikarwar B, Sachdeva G. Experimental investigation of double-glazed double-pass solar air-heater (DG-DPSAH) with multi-v ribs having trapezoidal roughness geometry. J Ther Eng 2023;9(5):1228–1244.

INTRODUCTION

The impact of increased environmental pollution has compelled mankind to search for new options of sustainable resources. Green resources such as solar, wind, biomass, geothermal, and so on are the new hope for the future as new energy avenues [1]. Renewable energy such as solar energy can be the "one in all" energy resource for meeting all countries energy crises and needs. Solar energy is utilized via mankind using various devices such as solar collectors [1], photovoltaic modules [2], solar ponds [3], solar cookers [4], solar air heaters (SAH) [5], etc. Among these devices, the solar air heater (SAH) is one of the promising

*Corresponding author.
*E-mail address: bssikarwar@amity.edu

and simplest solar thermal devices that utilize the heat energy of solar radiations to heat up the flowing air for drying process and heating of space. Many studies [5-7] have used the flat plate model for exchanging solar heat energy from plate to air in a solar air-heater.

In the SAH device, the thermal conductivity (~0.02588 W /mK at temperature 300 K) of the working fluid flowing through the duct is lower. Hence, these devices have poor efficacy. Besides low conductivity, other aspects that contribute to the lower efficiency of solar air-heater are large thermal inertia of the absorber plate, geometric constraints, thermal losses, and time-dependence over solar radiation [7,8]. With advancement of technology in fabrication, many changes and up-gradations were carried out to alter the roughness of absorber plate in solar air heater such as incorporation of longitudinal fins [9], increased number of passes [10,11] and conical surfaced absorber layer [12]. Chabane et al. [9] investigated the thermal performance of a single-pass solar air-heater roughened with longitudinal fins at mass flow rate of 0.012 kg/s and 0.016 kg/s respectively. Khanlari and Gungor [10] focused more on the aspect of triple-pass and quadruple-pass solar air-heater for enhancing the effectiveness of SAH for a V-grooved absorber plate. Phu et al. [11] assessed the effect of triple-pass airflow in a solar air-heater for Reynolds number varying from 8000 to 18000. Abuska [12] focused on different shapes of absorber plate, namely, conical and flat in a SAH to determine the average thermal and exergy efficiency in outdoor conditions at mass flow rate of 0.04, 0.08 and 0.10 kg/s. In addition, many researchers have focused more on the aspect of double-pass [10] and triple-pass solar air-heater [11] for enhancing the effectiveness of SAH. In addition, several experimental [12,13] and theoretical studies [14] were carried out to enhance the performance of SAH such as altering the design of the duct, minimizing heat loss from the system, and creating turbulence in the path of air.

For enhancement of thermo-hydrodynamic performance of SAH, several researchers alerted the roughness of the absorber plate using artificial roughness in the form of ribs [15-18]. Saravanakumar et al. [15] presented a mathematical model for analysing the performance of a SAH roughened with arc-shaped ribs. Along with ribs, fins and baffles were also employed to increase the efficacy. Sahu and Prasad [16] theoretically analysed the thermal performance of solar air-heater artificially roughened with arc-shaped wire. Their results showed that the maximum efficiency was achieved at flow attack angle of 0.33° and e/D_h of 0.0422. Komolafe et al. [17] used rectangular ribs over absorber surface to investigate the thermal efficiency of SAH. The maximum thermal efficiency achieved was around 56%. Kumar and Layek [18] analysed the Nusselt number and fluid flow pattern for transverse circular rib roughened SAH. Their results interpreted that at roughness pitch ratio of 10, maximum heat transfer took place from the absorber plate to the air. Mahanand and Senapati [19] conducted thermal analysis over transverse inverted T-shaped roughened collector. The maximum

enhancement factor achieved was 1.86 at relative roughness height of 0.042, e/D of 0.042 and Re of 15000. Varshney and Gupta [20] tested the performance of solar air-heater roughened using rectangular sectioned tapered rib. These ribs were analysed for 12 different configurations having taper angle of 1.6°, 2.3° and 3.2°. At Re of 12000, P/e of 10.7 and taper angle of 1.6°, the maximum performance index found was 1.91. Saravanan et al. [21] performed experiment to study the flow characteristics for SAH having perforated and non-perforated staggered multi-C ribs. It was evident through results that the thermal performance of perforated ribs was slightly higher than that of non-perforated ribs. Wang et al. [22] carried out experiments to analyse the thermal efficiency of SAH having S-shaped ribs with gaps. The enhanced thermal efficiency obtained was 13% to 48% using the proposed roughness geometry. Parsa et al. [23] conducted parametric study over a solar air-heater having staggered cuboid baffles. Results interpreted that maximum thermo-hydraulic performance factor obtained was 3.43 at Re of 5080. Lanjewar et al. [24] experimented over a solar air-heater roughened with W-shaped ribs. Maximum Nusselt number enhanced was 2.36 times of smooth duct SAH for α of 60°, Re of 14000 and e/D of 0.03375. Patil et al. [25] conducted thermohydraulic analysis to test the performance of solar air-heater roughened using discretized broken V-ribs. Results interpreted increase n the heat transfer rate when compared to V-ribs having gap. Jin et al. [26] numerically investigated the heat transfer characteristics of a multi-V ribbed solar air-heater. The maximum thermo-hydraulic performance factor achieved was found to be 2.35 for this roughness arrangement. The staggered pattern of multigap V-down ribs was tested by Deo et al. [27] to predict the flow pattern and heat transfer rate. Maximum increment in Nusselt number was found to be 3.34 times of conventional SAH. Jin et al. [28] carried out numerical simulation for staggered multi-V ribbed solar air-heater. They showed that the maximum increment achieved was 18% and 25% for thermohydraulic performance factor and Nusselt number (Nu) for inline rib arrangement. Kumar et al. [29] focused augmentation of heat transfer of a SAH using discrete broken-V baffles. They observed maximum enhancement in performance for α of 60°, P/e of 1.5 and D/L_v of 0.67. Kashyap et al. [30] did parametric study for investigating the effect of multi-V with multi-symmetric gap roughened over the absorber plate of a SAH. They reported increment in Nusselt number by 6.46 times that of smooth solar air-heater. Hassan and Abo-Elfadl [31] conducted experiment over the double-pass and double-port solar air heater arrangement. The maximum thermal efficiency of pin finned absorber plate and flat plate absorber plate was found to be 79% and 70% respectively. Abo-Elfadl et al. [32] had compared the performance of tubular solar air-heater (TSAH) with the flat-plate solar air-heater (FSAH) having same dimensions and environmental conditions. It was found that the efficiency of TSAH was greater than the efficiency of FSAH by 40.3% at air flow rate of 0.025 kg/s. Singh [33] investigated the porous wavy wiremesh pattern for both single and double-pass solar

air-heater configuration. It was found that thermohydraulic performance of serpentine packed bed SAH was 24.33% better than the conventional flat-plate SAH. Ho et al. [34] improved the performance of solar air-heater using the combination of fins and baffles under the recycled air flow arrangement. Nowzari et al. [35] used the integrated packed bed and partially perforated cover for enhancing the thermal efficiency of SAH. The thermohydraulic study was conducted separately for single and double-pass SAH respectively.

Based on the literature, it can be concluded that the available artificial roughness over absorber plate of SAH gives rise to a higher heat transfer rate [27-30]. However, they increase friction factor more than the increase in heat transfer coefficient. In this manuscript, new roughness in the form of multi-V ribs having trapezoidal slots over absorber plate was fabricated for increasing the heat transfer rate between the plate and air. As per authors understanding, thermo-hydrodynamic performance for proposed morphology of absorber plate with double glazed-double pass air flow arrangement SAH is not reported explicitly till now. An experimental setup was designed and fabricated for knowing the efficacy of proposed roughness over absorber plate with respect to smooth plate. The experiments were conducted under Indian climatic conditions (Latitude = 28.53˚N and Longitude = 77.39˚E) for a week in the month of September and October. The results show that the thermo-hydraulic performance parameter ($Nu/f^{1/3}$) of the proposed roughness geometry is higher than the other shapes of roughness. Hence, combination of double-glass cover and double-pass arrangement with the proposed roughness geometry increases efficiency of the solar air heater at least by one order of the present system.

EXPERIMENTAL STUDY

The setup was built to perform the experimental study on double-glass with proposed absorber plate geometry/ smooth plate of SAH which have a double-pass air flow arrangement. Figure 1(a) shows the schematic diagram of the experimental setup; however, Figure 1(b) shows the
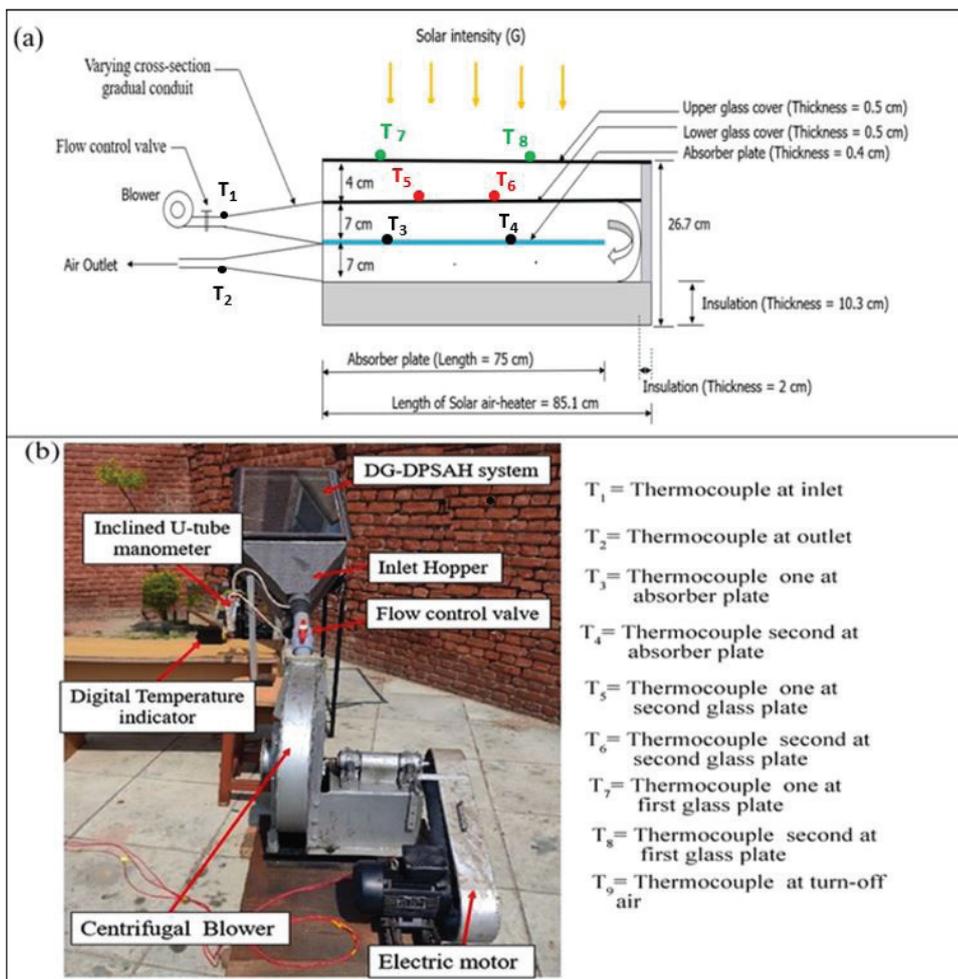
Figure 1. (a) Schematic diagram of DPSAH system (Side-View) and (b) photograph of experimental setup. Various positions of the thermocouples for measuring temperature of air inlet, air outlet, first glass plate, and second glass plate and air temperature of the air before entering the second passes.
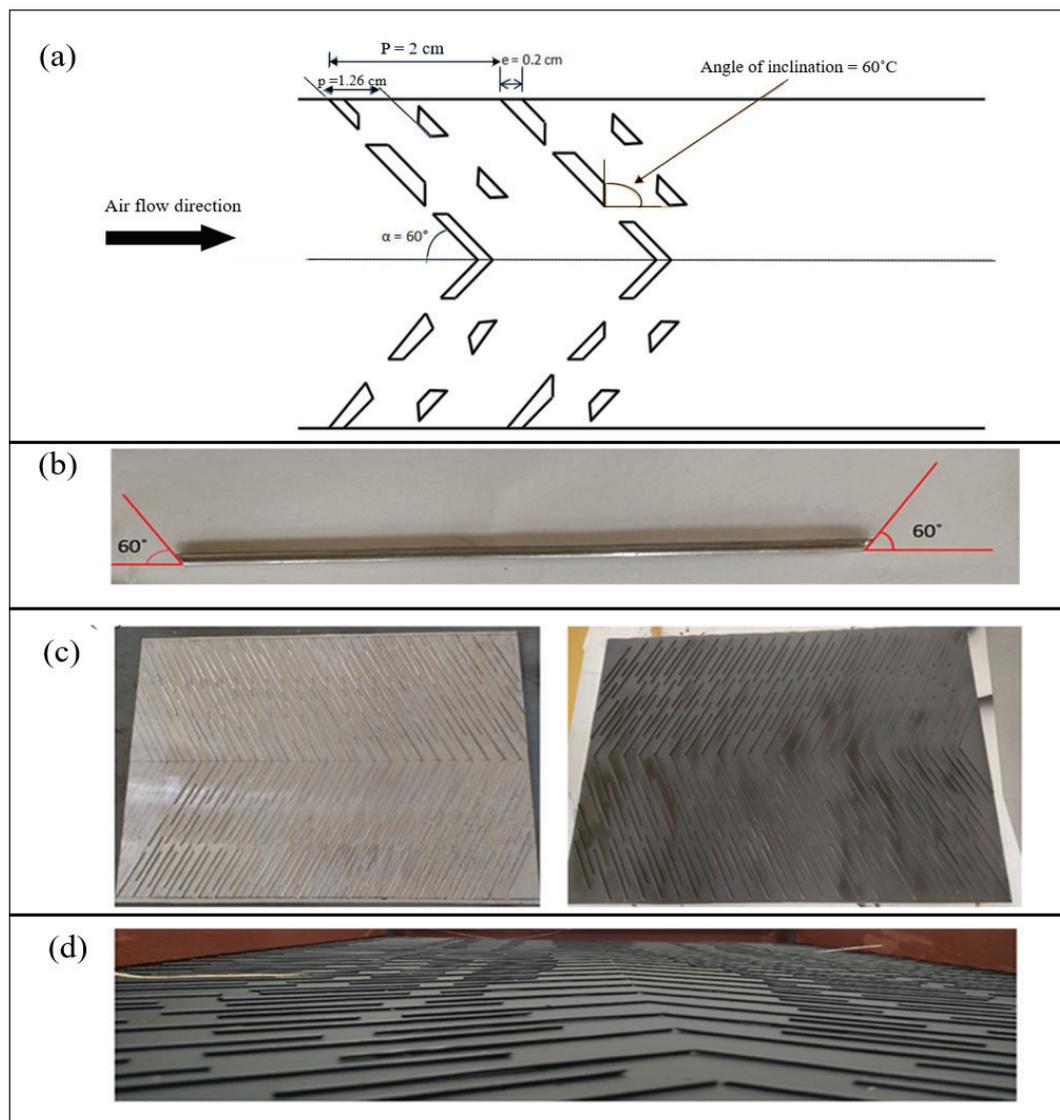
Figure 2. (a) Schematic diagram of new roughness geometry (Multi V-ribs with trapezoidal slot). (b) An aluminum circular wire having sharp trapezoidal corners cut at an angle of 60˚ on both sides. (c) Absorber plate with new roughness geometry and Matt black painted absorber plate with new roughness geometry. (d) Close view of absorber plate having new roughness geometry (Along with thermocouples attached over the plate).

photograph of the setup. This double-pass double-glass SAH (DPSAH) system consists of a rectangular box made up of wood having dimensions (L × W × H) 85.1 × 54 × 26.7 cm. The inlet, test and outlet region of the setup were designed and constructed as per ASHRAE 93 standards [36]. To minimize the heat loss from the DPSAH system to the surrounding, the whole frame was fabricated using thick wood of thickness 2 cm, as shown in Figure 1(a). In addition, the wall of the duct was insulated via black thermal insulation foam of thickness 3 cm. A centrifugal blower is used for air flow, and it was connected to the setup by varying cross-section gradual conduit.

The setup has two glass covers viz. upper glass cover and the lower glass cover of dimensions 80.7 × 48.7 cm

and 83.1 × 51.4 cm respectively having a thickness of 0.5 cm for entrapping more thermal radiations. An aluminum plate (75 cm× 49.5 cm× 0.4 cm) of the roughness of 25 μm was used as a smooth absorber plate, as shown in Figure 2. Similarly, an identical smooth absorber plate was used for creating new roughness geometry as shown in figure 2(a). For creating roughness, an aluminum wire of 2 mm diameter was cut into small pieces in the shape of a trapezoid with sharp ends, as shown in figure 2(b). These wires were fastened at an angle of attack of 60˚ over absorber plate using thermal glue as shown in Figure 2(c).

The absorber plate was painted matt black (Absorptivity = 95%) to increase the absorption rate of solar energy falling over it as illustrated in figure 2(d). The setup was installed at

Amity University, Noida, India having a latitude of 28.53˚N and longitude of 77.39˚E in the month starting from the end of September to the first week of October 2021. It was inclined at an angle of 28.5˚ which is equal to the latitude of Noida, India location and it was placed in south-facing orientation to receive the maximum solar intensity. Finally, the experimental studies were carried out for comparing the efficacy of the proposed absorber plate with respect to the smooth plate. Table 1 listed the geometrical parameters while table 2 listed the thermophysical properties of different components present in the setup.

Measuring Parameters

For the experimental study, different operating parameters were measured and noted down from 8:00 am to 16:00 pm. The temperatures were measured using calibrated K-type thermocouples which were mounted at nine different locations as shown in Figure 1(a) and they were calibrated with omega-thermometer before fixing up in the setup. The thermocouples were connected to a digital temperature indicator, while the airflow meter was calibrated with digital anemometer (Model: Work Zone AVM-03) before fixing. The solar intensity was registered using a solar meter of model 'Amprobe Solar-100 solar power meter'. A flow control valve was used to regulate the flow of working fluid at different mass flow rates and an inclined U-tube manometer was used to measure pressure

Table 1. Range of parameters of the DG-DPSAH

S.No.	Parameters	Range of values
1	Thermal conductivity of glass	0.075 W/mK
2	Thermal conductivity of insulation	0.036 W/mK
3	Number of gap (n)	2
4	Relative rib pitch (p/P)	0.63
5	Relative roughness pitch (P/e)	10
6	Angle of attack (α)	60°
7	Angle of inclination (Trapezoidal slot)	60°
8	Ambient temperature (Ta)	30° - 39°C
9	Solar irradiation (G)	403 - 960 W/m^2
10	Velocity of wind (V$_w$)	0.4 – 2 m/s
11	Air flow rate	0.026 – 0.078 kg/s

Table 2. Radiation properties of different components

S.No.	Components	Dimension (cm)			Transmissivity (τ)	Emissivity (ε)	Absorptivity (α)
		L	*b*	*h*			
1	Upper glass cover	83.1	51.4	0.5	0.95	0.92	0.05
2	Lower glass cover	80.7	48.7	0.5	0.95	0.92	0.05
3	Absorber plate	75	49.5	0.4	-	0.9	0.91
4	Matt black paint	-	-	-	-	0.9	0.95
5	Insulation	85.1	54	10.3	-	-	-

Table 3 (a). Components used for experimental analysis

S.No.	Components	Manufacturer Details
1	Glass cover	Manchanda Enterprises
2	Absorber plate	Shiv Shakti Enterprises
3	Matt black paint	Ambey Paints

drop through the setup. Further, the ambient temperature and velocity were measured using the anemometer. The manufacturer details of the components purchased for the present study is given by table 3(a). The specification of the measuring instrument used for the experimental analysis listed in Table 3 (b).

Table 3 (b). Components used for experimental analysis

S.No.	Components	Specification/Range	Model
1	K-type thermocouple	0 to 1024 ˚C	MAX6675
2	Digital Anemometer	0.3 – 30 m/s	Work Zone: AVM-03
3	Solar meter	0-2000 W/m^2	Amprobe Solar-100 solar power meter
4	Digital temperature indicator	0 to 95˚C	TC544C Digital temperature controller
5	U-tube manometer	0 to 50 mm, H$_2$O	Flowtech PM-6105
6	Flow control valve	15 to 150 PSI	T-BAY PVC

Efficiency of DPSAH

The double pass solar air heater (DPSAH) efficiency (η) is estimated as reported in the literature [37]

$$\eta = \frac{Q_o}{Q_{in}} \tag{1}$$

where, Q_{output} is the energy gain by air flow of absorber plate and is calculated using energy balance equation.

$$Q_o = \dot{m}c_p(T_3 - T_2) \tag{2}$$

where C_p is the specific heat of the working fluid in kJ/kg K.

Q_{input} is the input thermal energy rate [38] given by equation 4.

$$Q_i = G \times A \tag{3}$$

where G is the solar irradiation in W/m²

Using equation 2, the average heat transfer coefficient (h) is estimated. Hence. the average Nusselt number (Nu) is estimated as:

$$Nu = \frac{hD_h}{k} \tag{4}$$

Using digital anemometer data, the mass flow rate of the working fluid and corresponding Reynolds number (Re) are estimated as:

$$\dot{m} = \rho A V \tag{5}$$

$$Re = \frac{\dot{m}D_h}{A\mu} \tag{6}$$

where, ρ is the density of air, V is the average velocity of working fluid, A is cross section area of duct and D_h is hydraulic diameter of duct. However, the density of the working fluid is function of temperature and is estimated as [38]:

$$\rho = \frac{101.3}{0.287 \times T_1} \tag{7}$$

By knowing drop of pressure in duct from our experiment, the friction factor (*f*) of duct is estimated as:

$$f = \frac{\Delta P \, D_h}{2\rho L V^2} \tag{8}$$

The thermohydraulic performance factor (THF) is determined [39] from the following equation:

$$\text{THF} = \frac{Nu/Nu_s}{(f/f_s)^{1/3}} \tag{9}$$

The heat loss (Q_{loss}) from the upper glass plate [40] is determined using

$$Q_{loss} = \frac{T_{gu} - T_a}{\frac{1}{Ah_w - Ah_{r,0}}} \tag{10}$$

where T_{gu} is the average temperature of upper glass cover and T_α is the ambient temperature in ˚C, h_w is the convection heat transfer coefficient due to ambient air speed in W/m²K and $h_{r,0}$ is the radiation heat transfer coefficient on the upper glass cover in W/m²K

The convection heat transfer coefficient due to ambient air speed [41] is determined using the formula:

$$h_w = 5.7 + 3.8 \, V_w \tag{11}$$

where V_w is the ambient air velocity in m/s

The radiation heat transfer coefficient [42] is given by the equation:

$$h_{r,0} = \frac{\sigma\epsilon_g(T_g + T_s + 546)\left((T_g + 273)^2 + (T_s + 273)^2\right)(T_g - T_s)}{T_g - T_s} \tag{12}$$

where σ is the Stefan Boltzmann constant, ϵ_g is the emissivity of glass cover and T_s is the sky temperature (˚C). The sky temperature is determined [43] using the formula:

$$T_s = 0.0522 \, (T_a + 273)^{1.5} - 273 \tag{13}$$

The equation 10-13 were used for estimating the useful energy gain from this system.

Experimental procedure and calculations: The experiments were conducted for selected range of operating factors and accordingly, desired data was fetched to calculate the energy gain, pressure drop, and efficiency. The parameters that were considered constant before experimentation includes:

- Air mass flow rate (0.026 kg/s, 0.052 kg/s, and 0.078 kg/s)
- Roughness parameters of multi-V ribs having trapezoidal slots

[Relative rib pitch (p/P) =0.063, Relative roughness pitch (P/e) =10, angle of attack=60˚ and angle of inclination of trapezoidal slot=60˚]

Following parameters were registered each hour to calculate the overall output from the system.

i. Temperature of the working fluid at the inlet and outlet section of the setup was recorded on an hourly basis.
ii. The average temperature of the absorber plate, lower glass cover, and upper glass cover was recorded.
iii. The external parameters such as ambient temperature, velocity, and solar radiation were recorded each hour.
iv. Pressure losses inside the inlet and outlet section were recorded.

RESULTS AND DISCUSSION

The experiments were conducted for a week (from 30/09/2021 to 6/10/2021) and throughout this week, the climatic conditions were almost similar. Figure 3 shows the flow pattern created by the present roughness geometry. Figure 4 (a) shows the outlet air temperature results of the double-glazed DPSAH for smooth absorber plate while figure 4(b) shows the outlet air temperature results of the double-glazed DPSAH for roughened absorber plate. Additionally, the variation of solar intensity and ambient temperature concerning time is also depicted in figure 5. The result indicates that the recorded temperature of outlet air increases rapidly starting from morning and reaches the peak point before noon. Afterward, the temperature readings drop concerning time following a similar pattern of the solar intensity. The main point noted here is that the maximum solar intensity occurs before the DG-DPSAH reaches the peak temperature. The occurrence of lag between the timeline of the peak temperature and maximum solar intensity recorded may be due to the time taken by DG-DPSAH to heat the absorber plate and air. The lower glass plate temperature is greater than the upper glass plate temperature and the latter is greater than the ambient air temperature due to the transfer of solar energy from the ambient to the glass plate. As expected, the absorber plate temperature is greater than the lower glass plate temperature due to concentrated heat energy falling over the absorber plate from the lower glass plate. On comparison of results of figure 4(a) with the corresponding figure 4(b), it is found that the outlet air temperature is greater in the case of DG-DPSAH for roughened absorber plate than that of DG-DPSAH for smooth absorber plate. As the roughness geometry creates a drift in the flow region, breakdown occurs in the viscous sub-layer; thereby, increasing the intensity of heat transfer

from the absorbing surface to the air. In addition to this, losses to the environment are reduced as lower glass plate reduces the amount of solar radiation reflecting back to the ambient. Hence, due to double glazing, more radiations are entrapped by the twin glass ceiling. This results in increased outlet air temperature from the DPSAH system. The maximum air temperature of the outlet section is 49°C for DG-DPSAH with smooth absorber plate and 53.6°C for DG-DPSAH with roughened absorber plate. This shows that there is an increase of 4.6°C in the outlet air temperature due to the attachment of new roughness geometry over the absorbing plate. This explains that roughness positively impacts the output of the DG-DPSAH as this roughness pattern gives more surface area to the air passing through it. In addition, it generates more mixing of fluid by void formation and secondary flow. Therefore, promoting proper scattering of primary flow and resulting into faster mixing of the fluid in the wake region.

The percentage increase in outlet air temperature of the DG-DPSAH with roughened absorber plate compared to DG-DPSAH with smooth absorber plate is 3.2%, 4.7%, and 10.3% at a mass flow rate of 0.026 kg/s, 0.052 kg/s, and 0.078 kg/s, respectively. This implies that with an increase in air MFR inside the duct, there is an increase in outlet air temperature. It also means that the temperature of the absorber plate and lower glass cover decreases with an increase in the mass flow rate of the working fluid.

Rate of Heat Transfer in form of Actual Energy Gain

This section presents the results of energy gain by each DG-DPSAH system on an hourly and daily basis.

(a) *Hourly energy gain*: The variation in hourly energy gain by the DG-DPSAH system is calculated from equation (3) for DG-DPSAH with smooth absorber plate and DG-DPSAH with roughened absorber plate at different
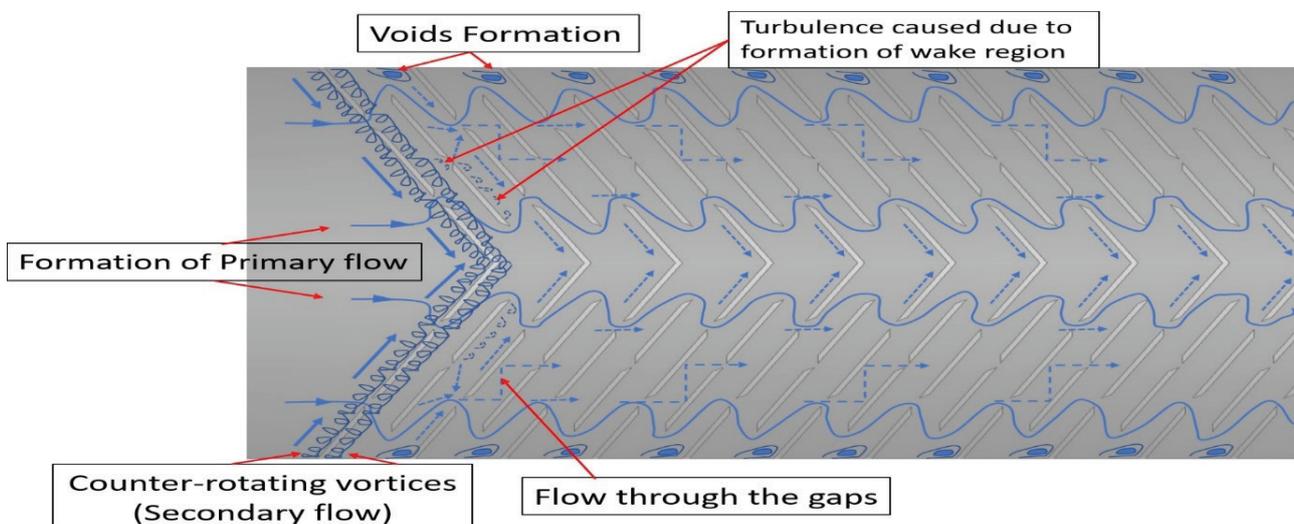
Figure 3. Flow pattern for multi-V ribs with trapezoidal slots (showing reattachment of primary flow and generation of secondary vortices as counter rotating stream near the wall of trapezoidal sides).
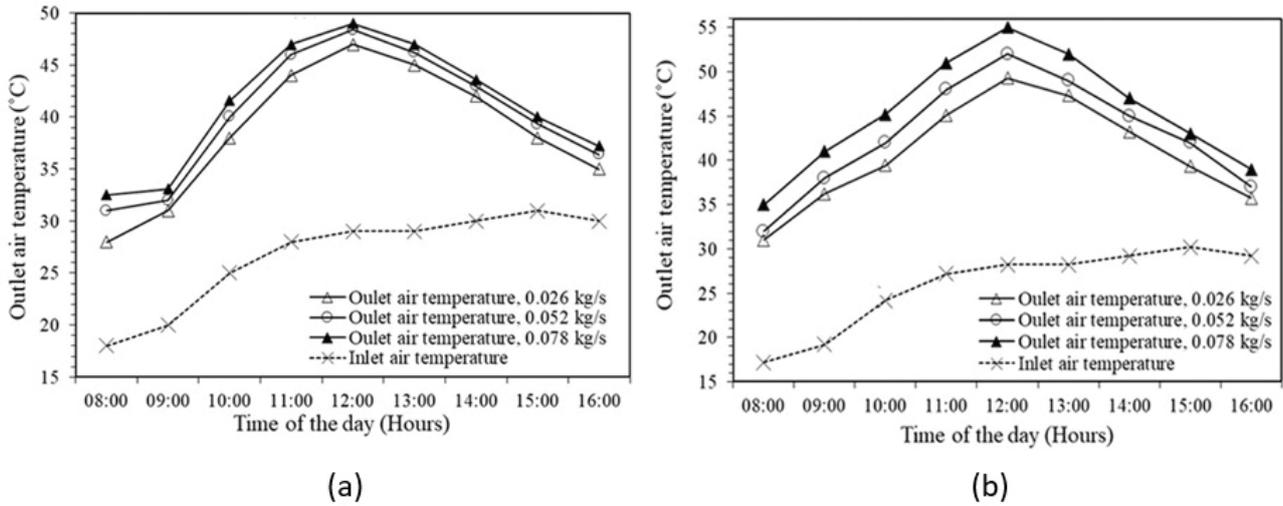
Figure 4. Variation of outlet air temperature with respect to time. (a) DG-DPASH for smooth absorber plate and date of the experiment is 5th October 2021 and (b) DG-DPASH for roughened absorber plate and date of experiment is 6th October 2021 (As per our measurement, the environmental conditions for 5th October 2021 and 6th October 2021 are approximately same. Look out 'India Meteorological Department' data (https://mausam.imd.gov.in) for authenticity of these data regarding climate condition).
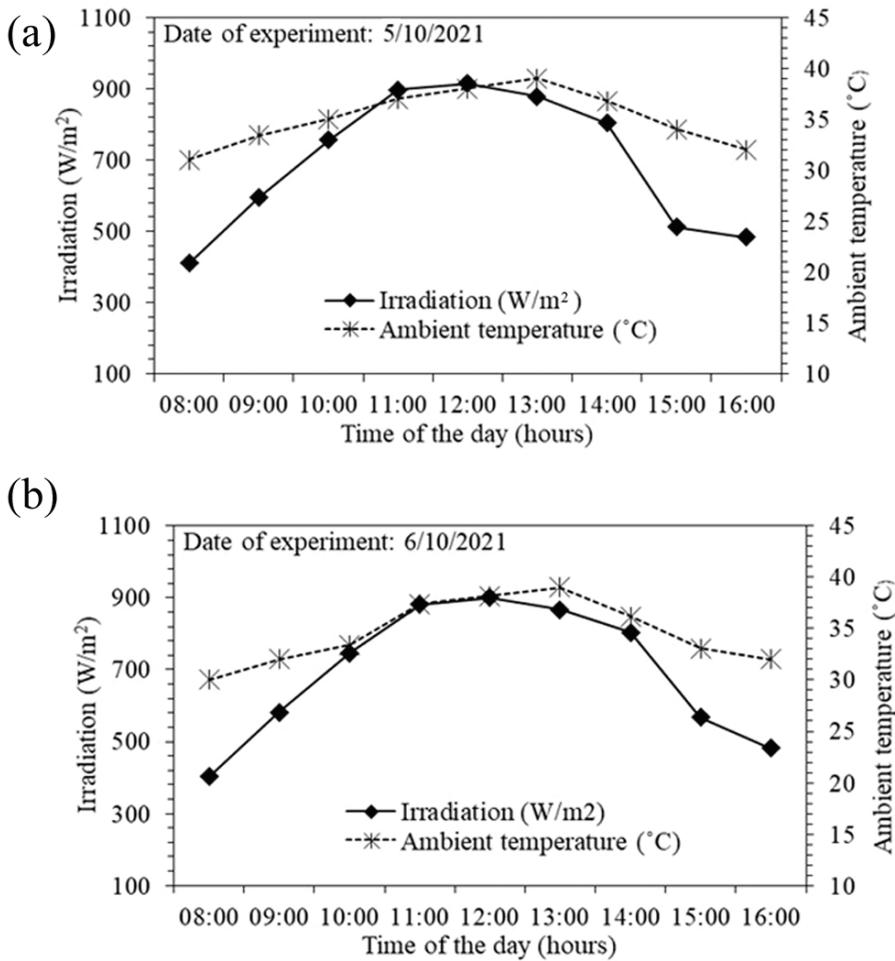
Figure 5. Variation of irradiation and ambient temperature with respect to time recorded on (a) 5th October 2021 and (b) 6th October 2021.
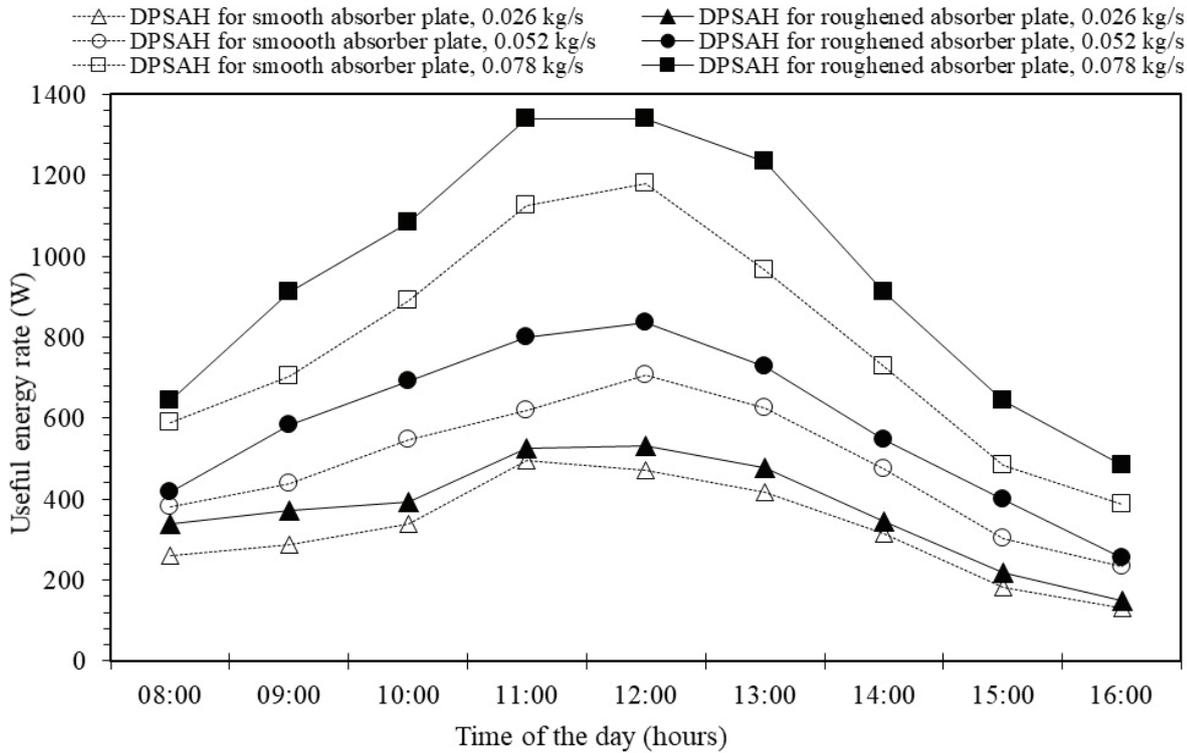
Figure 6. Variation of useful energy rate with respect to time.

MFRs as shown in figure 6. The graph shows that the hourly energy gain follows the same pattern similar to ambient temperature, outlet air temperature, and solar intensity which reaches its peak point between 12:00 pm to 13:00 pm, then it gradually reduces with time. The main factor that determines the actual thermal energy gain is the air temperature at the outlet section and this fact is pretty much verified by the equation (3). At a mass flow rate of 0.026 kg/s, 0.052 kg/s, and 0.078 kg/s, the maximum rise in actual energy gain for the DPSAH with roughened absorber plate compared to DG-DPSAH with smooth absorber plate is 18.2%, 20.3%, and 26.6% respectively.

(b) *Average useful energy gain:* Figure 7 shows the average energy rate increment with an increase in the mass flow rate of the working fluid. The reason behind this is the improved convective heat transfer coefficient of the absorber surface for DG-DPSAH system. The improvement shown by DG-DPSAH with roughened absorber plate over DG-DPSAH with smooth absorber plate in daily energy gain is around 18.2%, 20.3%, and 26.6% at 0.026 kg/s, 0.052 kg/s, and 0.078 kg/s respectively. In other words, it can be said that the accumulated heat gain from the absorbing surface to the working fluid for the DG-DPSAH with roughened absorber plate is better than DG-DPSAH with smooth absorber plate.
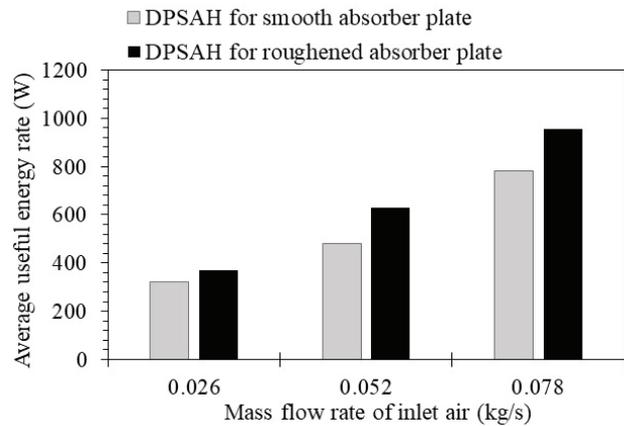
Figure 7. Variation of average useful energy rate with respect to time.

Thermal Performance

Thermal performance in the form of overall efficiency represents the actual output from the solar collector, it also indicates towards enhancement techniques required to improve the efficiency.

(a) *Hourly thermal efficiency:* Figure 8 shows the transformation of the hourly thermal efficiency of the DG-DPSAH for roughened absorber plate and DG-DPSAH for smooth absorber plate at different

mass flow rates with respect to time. The graph clearly shows that the thermal efficiency of both DG-DPSAHs with respect to lower mass flow rate rises slowly starting from morning till midday. This increase in efficiency is due to the increased rate of solar intensity. Between 12:00 pm to 13:30 pm, the efficiency rises continuously despite decreasing solar intensity. This may be due to enough solar energy grabbed by the DG-DPSAH body till midday which contributes positively towards thermal efficiency rise. After this point, as the solar radiation starts decreasing, the efficiency too starts reducing with time. At the same time, at a higher mass flow rate (0.078 kg/s), the thermal efficiency of each DG-DPSAH increases proportionally with time till 13:00 pm, then, it gradually decreases with time owing to reducing solar radiation value. Also, the increased convection rate due to the rising mass flow rate has a negative impact on the stored energy inside the DG-DPSAH body and therefore, efficiency deteriorated. The maximum thermal efficiency went up to 82.2% for DG-DPSAH with roughened absorber plate and 78.32% for DG-DPSAH with smooth absorber plate at 0.078 kg/s. This means that there is an increment of 54.74% and 49.86% for DG-DPSAH with roughened absorber plate and DG-DPSAH with smooth absorber plate respectively. It implies that the increment in thermal efficiency for mass flow rate of 0.078 kg/s is more than its increment at mass flow rate of 0.026 kg/s.

(b) *Average thermal efficiency:* Figure 9 (a) demonstrates the average thermal efficiency of DG-DPSAH with smooth absorber plate and DG-DPSAH with roughened absorber plate at different mass flow rates. The average daily thermal efficiency of DG-DPSAH with roughened absorber plate reaches up to 83.89%, while it reaches 74.44% in the case of DG-DPSAH with smooth absorber plate at a mass flow rate of 0.078 kg/s respectively. The average thermal efficiency for DG-DPSAH with roughened absorber plate is 55.3%, 65.67% and 83.89% for mass flow rate of 0.026 kg/s, 0.052 kg/s and 0.078 kg/s. On the other hand, it is 43.4%, 56.2% and 74.44% for DG-DPSAH with smooth absorber plate at 0.026 kg/s, 0.052 kg/s and 0.078 kg/s respectively. The results confirm the fact that DG-DPSAH with roughened absorber plate rises the convective heat transfer coefficient which results in increased energy output out of the system. Moreover, DG-DPSAH efficiency is maximum for a mass flow rate of 0.078 kg/s due to a higher flow rate.

Pressure Loss

Resistance to the flow of working fluid in the form of pressure drop is also one of the deciding factors in influencing the efficacy of a DG-DPSAH system. It is clear from the previous section results that energy gain from the DG-DPSAH increases with increasing air mass flow rate. Although, it also results in an increase in pressure drop of the working fluid as shown by figure 9 (b). It is also evident from the graph that pressure drop across DG-DPSAH with roughened absorber plate is more than DG-DPSAH with smooth absorber plate and the pressure drop elevates in DG-DPSAH with an increase in air mass flow rate. On comparison, it was found that the pressure drop across DG-DPSAH with roughened absorber plate is higher by 43.1%, 42.6%, and 54.3% compared to DG-DPSAH with
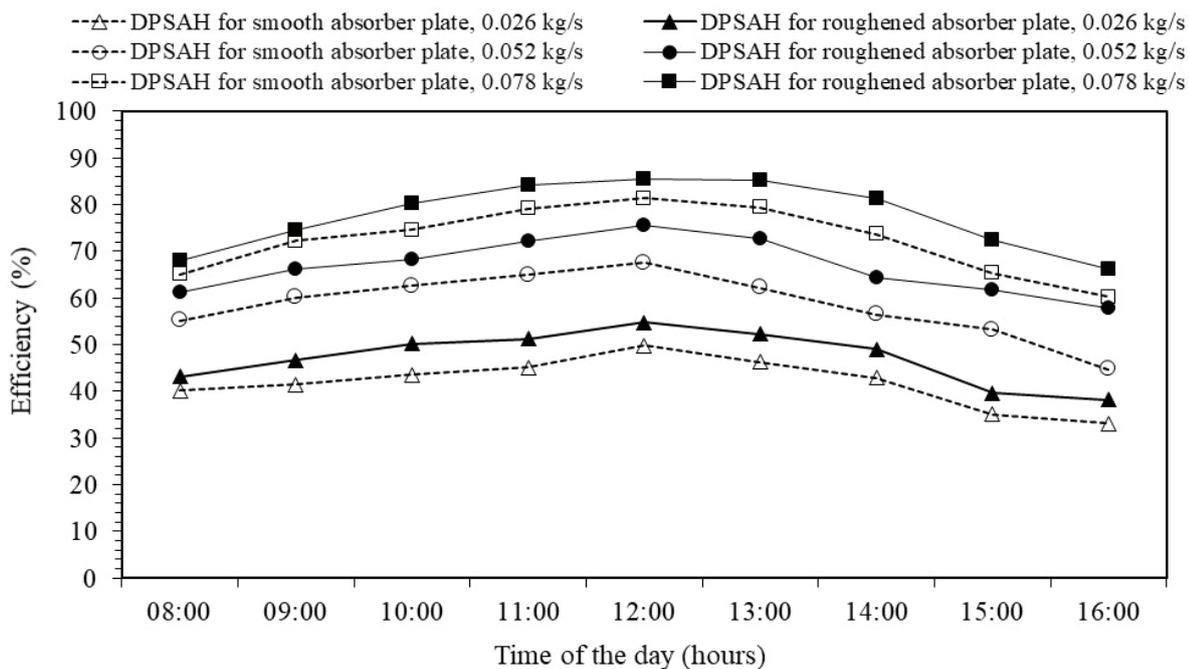
Figure 8. Variation of efficiency with respect to time.
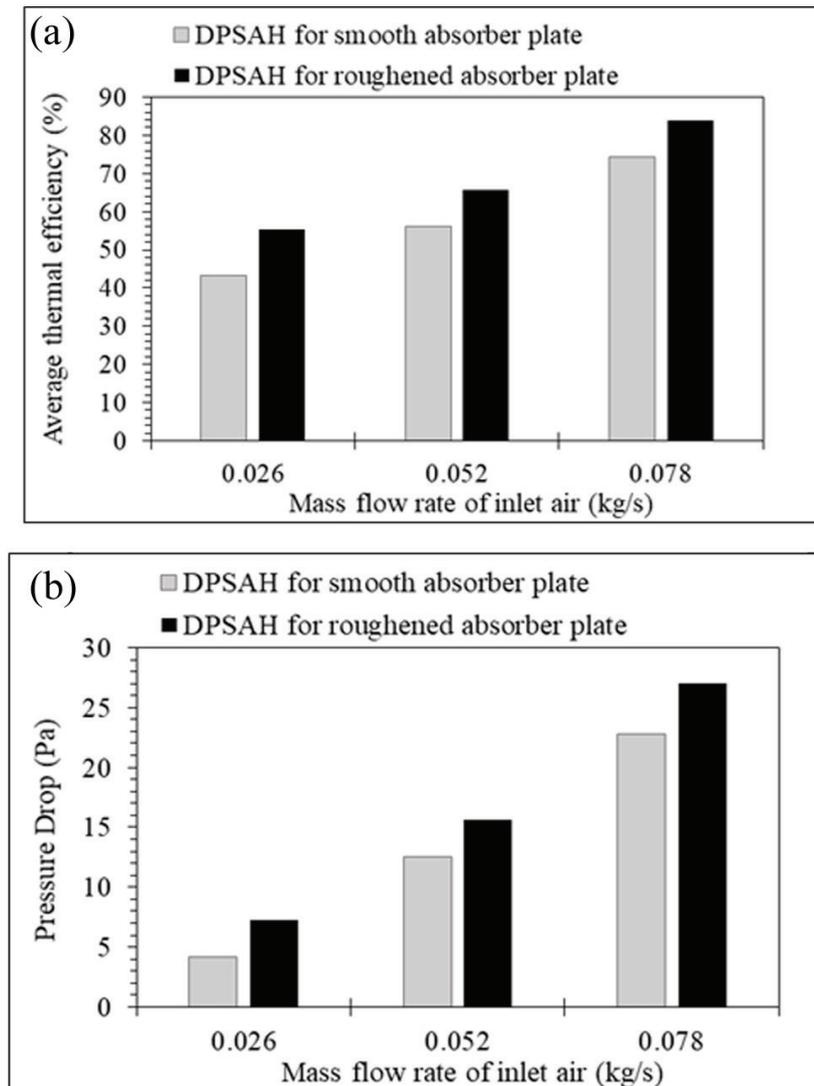
Figure 9 (a). Average thermal efficiency at different inlet mass flow rates and (b) Pressure drop at different mass flow rates through each DG-DPSAH.

smooth absorber plate for mass flow rate 0.026 kg/s, 0.052 kg/s, and 0.078 kg/s respectively.

Mass Flow Rate Effect

The mass flow rate of the working fluid impacts the energy gain, energy loss, outlet air temperature, pressure drop, and efficiency of both DPSAHs as depicted in table 4. It is also evident from table 4 that increasing the MFR rises the energy gain, pressure drop, and efficiency but at the same time, it also reduces the energy loss from the DPSAH system.

Table 4. Impact of mass flow rate on pressure drop and thermal efficiency

S.No.	SAH Configuration	Mass flow rate (kg/s)	Pressure drop (Pa)	Efficiency (%)
1.	DG-DPSAH for smooth absorber plate	0.026	4.2	43.4
	DG-DPSAH for roughened absorber plate		7.21	55.3
2.	DG-DPSAH for smooth absorber plate	0.052	12.5	56.2
	DG-DPSAH for roughened absorber plate		15.62	65.67
3.	DG-DPSAH for smooth absorber plate	0.078	22.8	74.44
	DG-DPSAH for roughened absorber plate		27.03	82.2

The results from the above-mentioned table show that the pressure drop is higher in DPSAH for roughened absorber plate as it creates turbulence. It also shows that the energy gain and efficiency of DPSAH for roughened absorber plate is more than DPSAH for smooth absorber plate. However, the total energy loss percentage in the case of DPSAH for smooth absorber plate is higher than DPSAH for roughened absorber plate.

Comparison of Thermal Efficiency with Previous Studies

The multi-V-ribs with trapezoidal slots gives more contact surface area to the air flowing through the duct compared to the previous roughness geometry of multi-V-ribs. Comparison of DPSAH performance with previously designed systems for the different mass flow rates is given in table 5. It is clear from the data that present proposed DPSAH is better than most of the SAH systems, while it is lower in efficiency when compared to tubular SAH.

The present design has higher thermal efficiency than the DPSAH having baffles and fins by 27% under almost similar ambient conditions. This difference in performance is due to the incorporation of new roughness geometry and double glass arrangement in the present design which subsequently enhances its output. However, DPSAH having a corrugated absorber surface has the same thermal efficiency as that of the present design but under different conditions

of mass flow rate and solar intensity. The operating conditions (G=1100 W/m², MFR=0.09 kg/s) of DPSAH having a corrugated absorber surface are much higher than that of the present design. This implies that the thermal efficiency of the DPSAH having a corrugated absorber surface for a mass flow rate of 0.076 kg/s and solar intensity of 915 W/m² (similar to operating conditions of the present design) would definitely be lower than 82%. Similarly, the thermal efficiency of DP serpentine wavy wire-mesh packed-bed SAH is lower than the present design by 9.975%. So, in short, it could be implied that the thermal performance of the present design is better in comparison to the previously designed solar collectors as the proposed roughness broke the trailing viscous layer form the surface and contribute towards creation of high turbulent factor into the flow domain.

Thermo-Hydraulic Performance Factor (THF)

The performance of the present artificial roughness geometry was compared with other similar configurations of V-ribs on the basis of Nusselt number, friction factor and thermohydraulic performance factor as shown in figure 10 (a), (b) and (c). Table 6 listed the performance factor of present study, discretized broken V-ribs, multiple V-shaped ribs and multigap V-down staggered ribs. These results were drawn for Reynolds number having value 5000, 10000

Table 5. Comparison of DG-DPSAH for roughened absorber plate with previous studies

S.No.	SAH Configuration	Mass flow rate (kg/s)	Maximum Irradiation (W/m²)	Maximum efficiency (%)
1.	DPSAH has a corrugated absorber surface (Hassan and Abo-Elfadl, 2018) [31]	0.09	1100	82
2.	TSAH (Abo-Elfadl et al., 2020) [32]	0.075	750	83.6
3.	DP serpentine wavy wire-mesh packed-bed SAH (Singh, 2020) [33]	0.05	900	74
4.	DPSAH has baffles and fins (Ho et al., 2012) [34]	0.077	830	60
5.	DPSAH has a perforated absorber plate (Nowzari et al., 2014) [35]	0.032	730	54.76
6.	Present study (DG-DPSAH for roughened absorber plate)	0.076	915	82.2

Table 6. Comparison of thermohydraulic performance factor of present study with other similar configuration of V-ribs for Re (5000, 10000 and 15000).

S.No.	Reynolds number	Thermohydraulic performance factor (TPF)			
		Present study (Multi V-shaped ribs with trapezoidal slot)	Patil et al. [25] (Discretized broken V-ribs)	Jin et al. [26] (Multiple V-shaped ribs)	Deo et al. [27] (Multigap V-down with staggered ribs)
1.	5000	2.23	1.71	1.53	2.09
2.	10000	2.31	2.07	1.84	2.21
3.	15000	2.62	2.43	2.05	2.45

and 15000. In these studies, the perceptible fact was the increase in thermohydraulic performance with increase in value of Reynolds number.

It is evident from the graph that present roughness has higher thermohydraulic performance as compared to other V-rib roughness geometry of solar air-heater due to the optimum rib inclination factor and trapezoidal slots that leads to generation of secondary flow between the adjacent ribs. These V-ribs with trapezoidal slots enhanced the heat transfer rate from the absorber surface to the working fluid. Hence, it can be said that the proposed roughness performs better than other similar artificial roughness geometries.
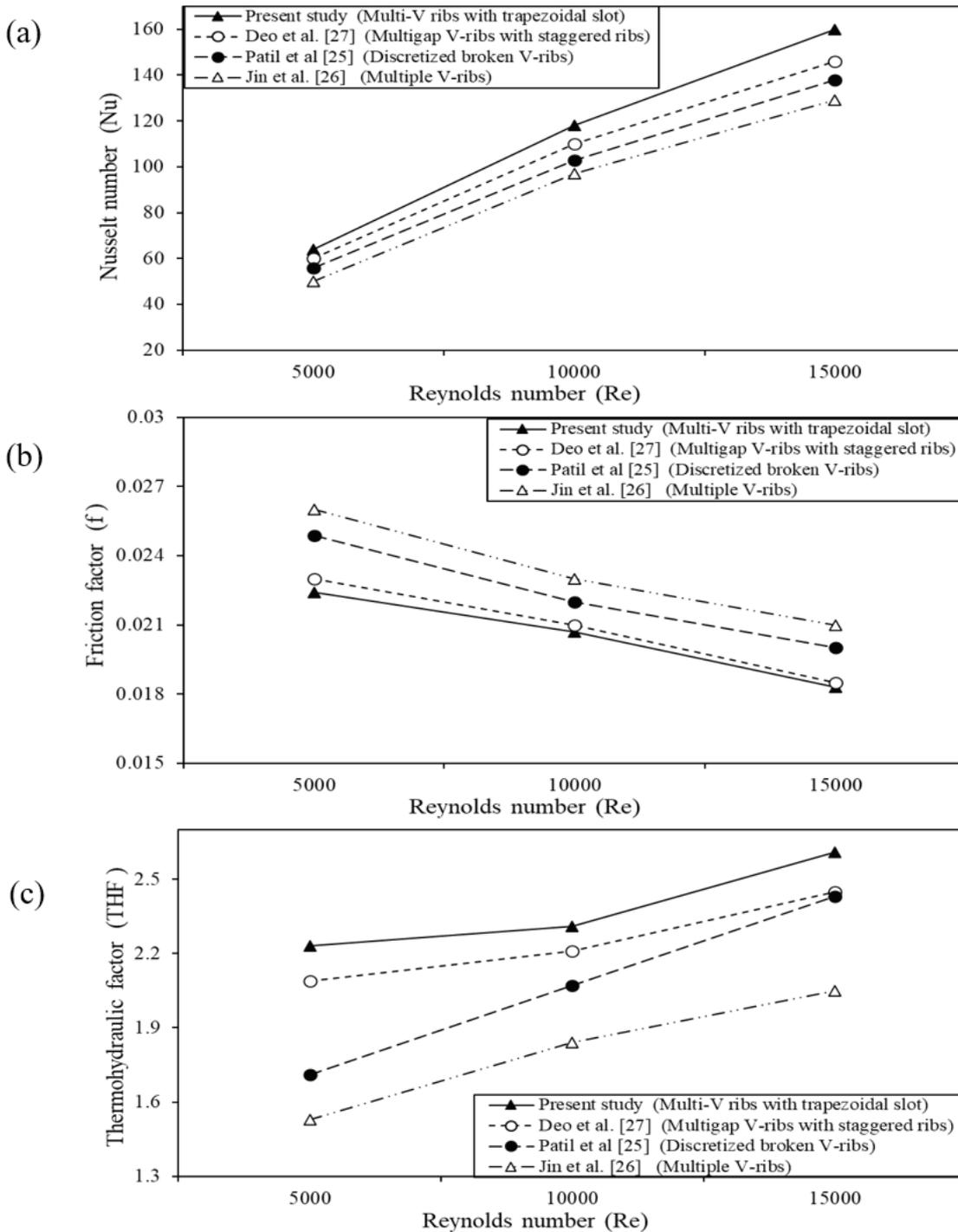
Figure 10. Comparison of (a) Nusselt number (b) friction factor and (c) thermohydraulic performance factor (THF) with Reynolds number for various configuration of similar ribs.

Uncertainty Analysis

In the experimental analysis, the errors and uncertainty of the measuring parameters were taken into consideration. Table-7 listed the uncertainty of the measuring instruments. The instruments including thermocouple, digital temperature indicator, anemometer, solar meter and manometer were calibrated before using in experiment to find out the relative error. On the basis of accuracy of each measuring device, the uncertainty in measurement was estimated following the procedure and formula mentioned by Taylor [44].

Table 7. Uncertainty of measuring instrument

S.No.	Device	Uncertainty (%)
1	Amprobe Solar-100 solar power meter (W/m²)	±2
2	K-type thermocouples (˚C)	±1.5
3	Digital temperature indicator (˚C)	±0.5
4	Anemometer (m/s)	±0.1
5	Inclined U-tube manometer (mm)	±1

The uncertainty (δ_z) is calculated using the formula [44]:

$$\delta_z = \left[\left(\frac{\partial z}{\partial x}\right)^2 \delta_x^2 + \left(\frac{\partial z}{\partial y}\right)^2 \delta_y^2\right]^{\frac{1}{2}} \tag{14}$$

where, z denotes the calculated values through collected experimental data. x & y denotes the measured values during experimental study.

Using Equation 14, the uncertainty of the energy gain and efficiency of the double-glazed double-pass SAH is estimated and its value is 2.8% and 2.4% respectively.

CONCLUSION

From the discussions part, the following findings could be drawn.

• The results cleared that DG-DPSAH for roughened absorber plate has greater outlet air temperature, higher useful energy gain, and higher thermal efficiency compared to DG-DPSAH for smooth absorber plate. Also, the present device has greater efficiency than the previously designed SAH system. The average increase in thermal efficiency of DG-DPSAH for roughened absorber plate is 53.2% and of DG-DPSAH for smooth absorber plate is 42.6% respectively.

• The useful energy gain reaches the maximum value for each DG-DPSAH system between 11:30 pm to 1:30 pm. It seems that useful energy gain is much more than the energy losses for this duration of the day.

• The value of solar irradiation and ambient temperatures impacts the performance of the DG-DPSAH system

as the temperature of output air at different mass flow rates from the system is directly proportional to the solar intensity. The result shows that the output air temperature lies between 41.6˚C to 52˚C for DPSAH with roughened absorber plate and 39.4˚C to 48.6˚C in the case of the DPSAH with smooth absorber plate for peak value of solar irradiation.

• Double-glass cover enhances the performance of the solar air-heater device as the maximum efficiency obtained by the DG-DPSAH is 82.2% in comparison to the maximum thermal efficiency obtained by a DPSAH (η=60%). This clears that the double glass cover with a gap of 4 cm from each other traps higher solar radiation and minimizes the losses of solar radiation from the glass cover.

• The value of maximum pressure drop for the DG-DPSAH with roughened absorber plate due to sharp edges in the form of trapezoidal corners inclined at 60˚angle of inclination is 27.03 Pa at air mass flow rate of 0.078 kg/s. The pressure drop of DG-DPSAH with roughened absorber plate is 15.64 % to 41.74% more than the DG-DPSAH with smooth absorber plate.

• Mass flow rate impacts the performance of DG-DPSAH system and maximum flow rate corresponds to a maximum value of useful energy gain, output air temperature and thermal efficiency, and vice-versa.

• A considerable increase in Nusselt number can be obtained by using multi-V ribs having trapezoidal slot due to increased surface area of ribs. The shape of the present roughness provides a systematic heat transfer through the spanwise distribution created by the geometry of trapezoidal slot. So, this leads to development of boundary layer phenomena and creation of turbulence which ultimately gives rise to flow separation and formation of secondary flow inside the flow domain; thereby, enhancing the heat transfer rate. The maximum increment achieved in the value of thermohydraulic performance factor (THF) was 2.62 for the proposed roughness geometry corresponding the Reynolds number of 15000.

Further studies could be carried out on the multi arc-shaped ribs with trapezoidal slots to analyze the flow pattern. Plus, a numerical study could be done on calculating and selecting the best-designed geometry of multi arc-shaped ribs at different inclination angles. In a future paper, we will analyze the efficacy of solar air-heater having multi-V ribs with trapezoidal slots alongside PV panels.

NOMENCLATURE

A	Surface area (m²)
C_P	Specific heat capacity of air (J/kg K)
D_h	Duct hydraulic diameter (m)
G	Solar irradiation (W/m²)
ΔT	Temperature difference across the duct (˚C)

e	Rib height (m)
f	Friction factor of roughened duct (-)
f_s	Friction factor of smooth duct (-)
h_w	Convective heat transfer coefficient due to ambient air speed (W/m^2K)
$h_{r,o}$	Radiative heat transfer coefficient on the upper glass cover (W/m^2K)
H	Convective heat transfer coefficient (W/m^2K)
$\dot{m}$	Mass flow rate (kg/sec)
ΔP	Pressure drop across duct (Pa)
p	Distance of staggered rib from V-rib (m)
P	Pitch of the rib (m)
Q_i	Input energy rate (W)
Q_{loss}	Rate of heat loss from the system (W)
Q_o	Energy gain by the system (W)
T_2	Outlet air temperature (˚C)
T_3	Temperature at point 3 over absorber plate (˚C)
T_4	Temperature at point 4 over absorber plate (˚C)
T_5	Temperature at point 5 over lower glass plate (˚C)
T_6	Temperature at point 6 over lower glass plate (˚C)
T_7	Temperature at point 7 over upper glass plate (˚C)
T_8	Temperature at point 8 over upper glass plate (˚C)
T_9	Temperature of return air (˚C)
T_{gu}	Average temperature of Upper glass cover (˚C)
T_{gl}	Average temperature of Lower glass cover (˚C)
T_a	Ambient temperature (˚C)
T_s	Sky temperature (˚C)
V	Velocity of air (m/s)
V_w	Ambient velocity (m/s)

Non-dimensional Number

Nu	Nusselt number of roughened duct
Nu_s	Nusselt number of smooth duct
Re	Reynolds Number

Greek Symbols

α	Angle of attack
ρ	Density of air (kg/m^3)
σ	Stefan Boltzmann constant
∈g	Emissivity of glass cover
η	Efficiency

Abbreviation

DPSAH	Double-pass solar air-heater
SAH	Solar air-heater
TSAH	Tubular solar air-heater
DG-DPSAH	Double-glazed double-pass solar air-heater
MFR	Mass flow rate
AR	Artificial roughness
THF	Thermohydraulic performance factor

CREDIT AUTHORSHIP CONTRIBUTION STATEMENT

Swati Mor: Conceptualization, Methodology, Investigation, Data curation, Resources, Writing- original draft. **B.S. Sikarwar:** Supervision, Conceptualization, Methodology, Writing- review & editing, Resources, Project administration. **Niraj Kumar:** Conceptualization, Methodology, Resources, Supervision, Writing- review. **Gulshan Sachdeva:** Writing- review & editing.

DECLARATION OF COMPETING INTEREST

The authors declare that they have no known competing interests or personal relationships that could have appeared to influence the work reported in this paper.

AUTHORSHIP CONTRIBUTIONS

Authors equally contributed to this work.

DATA AVAILABILITY STATEMENT

The authors confirm that the data that supports the findings of this study are available within the article. Raw data that support the finding of this study are available from the corresponding author, upon reasonable request.

CONFLICT OF INTEREST

The authors declare no potential conflicts of interest with respect to the research, authorship, and/or publication of this article.

ETHICS

There are no ethical issues with the publication of this manuscript.

REFERENCES

[1] Garg HP. Solar energy: Fundamentals and Applications. New York: Tata McGraw-Hill Education; 2000.

[2] Kumar D, Mishra P, Ranjan A, Dheer DK, Kumar L. A simplified simulation model of silicon photovoltaic modules for performance evaluation at different operating conditions. Optik 2020;204:164228. [CrossRef]

[3] Ali MM, Ahmed OK, Abbas EF. Performance of solar pond integrated with photovoltaic/thermal collectors. Energy Rep 2020;6:3200-3211. [CrossRef]

[4] Kreider JF, Keith F. Solar energy handbook. J Sol Energy Eng 1981;103:362−363. [CrossRef]

[5] Mor S, Kumar N, Sikarwar BS, Sachdeva G. Thermo-hydraulic analysis of a solar cogeneration air-heater. J Phys Conf Ser 2022;2178:012026. [CrossRef]

[6] Ansari M, Bazargan M. Optimization of flat plate solar air heaters with ribbed surfaces. Appl Therm Eng 2018;136:356−363. [CrossRef]

[7] Sureandhar G, Srinivasan G, Muthukumar P, Senthilmurugan S. Performance analysis of arc rib fin embedded in a solar air heater. Therm Sci Eng Prog 2021;23:100891. [CrossRef]

[8] Yadav AS, Thapak MK. Artificially roughened solar air heater: A comparative study. Int J Green Energy 2016;13:143−172. [CrossRef]

[9] Chabane F. Experimental study of heat transfer and thermal performance with longitudinal fins of solar air heater. J Adv Res 2014;5:183−192. [CrossRef]

[10] Khanlari A, Gungor A. Drying municipal sewage sludge with v-groove triple-pass and quadruple-pass solar air heaters along with testing of a solar absorber drying chamber. Sci Total Environ 2020;709:136198. [CrossRef]

[11] Phu NM, Tu NT, Hap NV. Thermohydraulic performance and entropy generation of a triple-pass solar air heater with three inlets. Energies 2021;14:6399. [CrossRef]

[12] Abuska M. Energy and exergy analysis of solar air heater having new design absorber plate with conical surface. Appl Therm Eng 2017;1313:115−124. [CrossRef]

[13] Mor S, Khan MU, Kumar N, Sikarwar BS, Sachdeva G. Recent advances in performance-enhancing parameters of solar air-heater: A review. In: Niraj K, Szalay T, Rahui S, Jaesun L, Priyank S, (editors). Advances in Interdisciplinary Engineering. New York: Springer; 2021. p. 43−57. [CrossRef]

[14] Phu NM, Bao TT, Hung HN, Tu NT and Nguyen VH. Analytical predictions of exergoeconomic performance of a solar air heater with surface roughness of metal waste. J Therm Anal Calorim 2021;144:1727−1740. [CrossRef]

[15] Saravanakumar PT, Somasundaram D, Matheswaran MM. Thermal and thermo-hydraulic analysis of arc shaped rib roughened solar air heater integrated with fins and baffles. Sol Energy 2019;180:360−371.

[16] Sahu MK, Prasad RK. Thermohydraulic performance analysis of an arc shape wire roughened solar air heater. Renew Energy 2017;108:598−514. [CrossRef]

[17] Komolafe CA, Oluwaleye IO, Awogbemi O, Osueke CO. Experimental investigation and thermal analysis of solar air heater having rectangular rib roughness on the absorber plate. Case Stud Therm Eng 2019;14:100442. [CrossRef]

[18] Kumar A, Layek A. Nusselt number and fluid flow analysis of solar air heater having transverse circular rib roughness on absorber plate using LCT and computational technique. Therm Sci Eng Progr 2019;14:100398. [CrossRef]

[19] Mahanand Y, Senapati JR. Thermal enhancement study of a transverse inverted-T shaped ribbed solar air heater. Int Commun Heat Mass Transf 2020;119:104922. [CrossRef]

[20] Varshney L and Gupta AD. Performance prediction for solar air heater having rectangular sectioned tapered rib roughness using CFD. Therm Sci Eng Progr 2017;4:122−132. [CrossRef]

[21] Saravanan A, Murugan M, Sreenivasa Reddy M, Ranjit PS, Elumalai PV, Kumar P, et al. Thermohydraulic performance of a solar air heater with staggered C-shape finned absorber plate. Int J Therm Sci 2021;168:107068. [CrossRef]

[22] Wang D, Liu J, Liu Y, Wang Y, Li B, Liu J. Evaluation of the performance of an improved solar air heater with "S" shaped ribs with gap. Sol Energy 2020;195:89−101. [CrossRef]

[23] Parsa H, Saffar-Avval M and Hajmohammadi MR. 3D simulation and parametric optimization of a solar air heater with a novel staggered cuboid baffles. Int J Mech Sci 2021, 205: 106607. [CrossRef]

[24] Lanjewar A, Bhagoria JL, Sarviya RM. Heat transfer and friction in solar air heater duct with W-shaped rib roughness on absorber plate. Energy 2011;36:4531−4541. [CrossRef]

[25] Patil AK, Saini JS, Kumar K. Experimental investigation of enhanced heat transfer and pressure drop in a solar air heater duct with discretized broken V-rib roughness. J Sol Energy Eng 2015;137:021013. [CrossRef]

[26] Jin D, Quan S, Zuo J, Xu S. Numerical investigation of heat transfer enhancement in a solar air heater roughened by multiple V-shaped ribs. Renew Energy 2018;134:78−88. [CrossRef]

[27] Deo NS, Chander S, Saini JS. Performance analysis of solar air heater duct roughened with multigap V-down ribs combined with staggered ribs. Renew Energy 2015;91:484−500. [CrossRef]

[28] Jin D, Zuo J, Quan S, Xu S, Gao H. Thermohydraulic performance of solar air heater with staggered multiple V-shaped ribs on the absorber plate. Energy 2017;127:68−77. [CrossRef]

[29] Singh I, Vardhan S, Singh S, Singh A. Experimental and CFD analysis of solar air heater duct roughened with multiple broken transverse ribs: A comparative study. Sol Energy 2019;188:519−532. [CrossRef]

[30] Kashyap AS, Kumar R, Singh P, Goel V. Solar air heater having multiple V-ribs with Multiple-Symmetric gaps as roughness elements on Absorber-Plate: A parametric study. Sustain Energy Tech Assess 2021;48:101559. [CrossRef]

[31] Hassan H, Abo-Elfadl S. Experimental study on the performance of double pass and two inlet ports solar air heater (SAH) at different configurations of the absorber plate. Renew Energy. 2018;116:728−740. [CrossRef]

[32] Abo-Elfadl S, Hassan H, El-Dosoky MF. Study of the performance of double pass solar air heater of a newly designed absorber: An experimental work. Sol Energy 2020;198:479−489. [CrossRef]

[33] Singh S. Experimental and numerical investigations of a single and double pass porous serpentine wavy wire mesh packed bed solar air-heater. Renew Energy 2020;145:1361−1387. [CrossRef]

[34] Ho C, Chang H, Wang R, Lin C. Performance improvement of a double-pass solar air heater with fins and baffles under recycling operation. Appl Energy 2012;100:155−163. [CrossRef]

[35] Nowzari R, Aldabbagh LBY, Egelioglu F. Single and double-pass solar air heaters with partially perforated cover and packed mesh. Energy. 2014;73:694−702. [CrossRef]

[36] ASHRAE Standard 93-77. Method of Testing to Determine the Thermal Performance of Solar Air Heater. New York: ASHRAE Standard; 1977. p. 1−34.

[37] Jin D, Xu S. Numerical investigation of heat transfer and fluid flow in a solar air heater duct with multi-V-shaped ribs on the absorber plate. Energy 2015;89:178−190. [CrossRef]

[38] Mahmood AJ, Aldabbagh LBY, Egelioglu F. Investigation of single and double-pass solar air heater with transverse fins and a package wire mesh layer. Energy 2015;89:599−607. [CrossRef]

[39] Webb RL, Eckert ERG. Application of rough surfaces to heat exchanger design. Int J Heat Mass Transf 1972;15:1647−1658. [CrossRef]

[40] John A, Duffie WAB. Solar Engineering of Thermal Processes. New Jersey: John Wiley & Sons; 2013. [CrossRef]

[41] Ansari M, Bazargan M. Optimization of flat plate solar air heaters with ribbed surfaces. Appl Therm Eng 2018;136:356−363. [CrossRef]

[42] Kalogirou SA. Solar Energy Engineering Processes and Systems. 2nd ed. U.K.. Elsevier Inc.; 2014.

[43] Soliman AMA, Hassan H. 3D study on the performance of cooling technique composed of heat spreader and microchannels for cooling the solar cells. Energy Convers Manag 2018;170:1−18. [CrossRef]

[44] Taylor JR. An Introduction to Error Analysis: The Study of Uncertainties in Physical Measurements. 2nd ed. New York: University Science Books; 1997.